Updated Constraints on Asteroid-Mass Primordial Black Holes as Dark Matter

Nolan Smyth,* Stefano Profumo, Samuel English, and Tesla Jeltema
Department of Physics, University of California, Santa Cruz and
Santa Cruz Institute for Particle Physics
(Dated: September 24, 2019)

Microlensing of stars places significant constraints on sub-planetary-mass compact objects, such as primordial black holes, as dark matter candidates. As the lens' Einstein radius in the source plane becomes comparable to the size of the light source, however, source amplification is strongly suppressed, making it challenging to constrain lenses with a mass at or below 10^{-10} solar masses, i.e. asteroid-mass objects. Current constraints, using Subaru HSC observations of M31, assume a fixed source size of one solar radius. Here we point out that the actual stars in M31 bright enough to be used for microlensing are much larger. We correct the HSC constraints by constructing a source size distribution based on the M31 PHAT survey and on a synthetic stellar catalogue, and by correspondingly weighing the finite-size source effects. We find that the actual HSC constraints are weaker in the primordial black hole mass, thus significantly broadening the range of masses for these as dark matter candidates.

I. INTRODUCTION

The miscroscopic nature of the dark matter (DM) permeating and shaping the observed universe remains mysterious. The persistent lack of a direct signal from weak-scale DM particle candidates has spurred growing interest in other possibilities. Primordial black holes (PBH), formed in the early universe as a result of large primordial density perturbations, are compelling DM candidates, if massive enough to survive Hawking evaporation over the age of the universe (i.e. if $m_{\rm PBH} \gg 10^{-17}\ M_\odot$). A variety of constraints, including but not limited to the effects of partial evaporation at low masses, and microlensing at larger masses, rule out PBH contributing 100% of the DM over most of the possible parameter space, roughly $5\times10^{-17} < m_{\rm PBH}/M_\odot < 10$. At present the only remaining window is towards the low-mass end, and, perhaps, at the solar-mass end, although the latter might be strongly constrained by CMB distortion caused by matter accretion onto the PBHs.

Here, we critically re-assess constraints in the most plausible region where PBH could be the DM, i.e. the asteroid-mass range $5 \times 10^{-15} < m_{\rm PBH}/M_\odot < 10^{-10}$. Over this mass range, the role of finite-size source effects is critical: as the Einstein radius of the lensing object in the source plane becomes comparable to, or larger than the source size, the source amplification from lensing is strongly suppressed. Ref. [1] showed that GRB femto-lensing constraints, after correction for finite-size effects, do not presently constrain PBH as DM candidates; Ref. [2] (see also [3]) realized their original constraints from optical observations of M31 had been vastly over-estimated because finite-source-size effects had originally not been accounted for. Ref. [4] re-assessed the effects, pointing out that even in the corrected version the assumed source size might have been underestimated, leading to incorrect, very optimistic constraints.

* nwsmyth@ucsc.edu

A. Microlensing Formalism

Gravitational lensing of astrophysical objects is one of the most powerful tools for observing dark, massive objects. For low-mass lenses, such as asteroid-mass PBHs, the images formed by gravitational lensing cannot be fully resolved. The result is that the source is magnified by a factor

$$A = \frac{\phi}{\phi_0}, \tag{1}$$

where ϕ_0 is the flux in the absence of lensing. The relevant scale for lensing by a PBH is the Einstein radius, R_E, which is defined as

$$R_E = \sqrt{\frac{4GM_{PBH}d_L(1-d_L/d_S)}{c^2}}, \tag{2}$$

where d_S and d_L are the distances between the observer and the source, and the observer and the lens respectively. The angular size of the Einstein radius is given by $\theta_E \equiv \frac{R_E}{d_L}$ and represents the angle between the source and its image as measured by an observer when the lens is directly between the observer and source.

If we ignore the effects of wave optics (the geometric optics approximation) then the magnification for a point source can be shown to be

$$A_{geo} = \frac{u^2+2}{u\sqrt{u^2+4}}, \tag{3}$$

where $\boldsymbol{\theta}$ is defined to be the angle of the source such that $u = \boldsymbol{\theta}/\theta_E$ is now the dimensionless impact parameter [5]. More formally, we can define the following dimensionless quantities

$$\mathbf{x} = \boldsymbol{\theta}_L/\theta_E, \quad \mathbf{y} = \boldsymbol{\theta}/\theta_E, \quad w = \frac{d_L d_S}{d_{LS}}\theta_E^2\omega, \tag{4}$$

where θ_L is the angular size of the lens, d_{LS} is the distance between source and lens, and θ_E is chosen to be the characteristic angle scale. We find the general amplification for the case of a spherically symmetric lens to be

$$A = -iwe^{\frac{iwy^2}{2}} \int_0^\infty xJ_0(wxy)e^{iw\left(\frac{x^2}{2}-\psi(x)\right)}dx, \qquad (5)$$

where J_0 is the zeroth order Bessel function. In the case of a point mass lens, which is an excellent approximation for a PBH, it can be shown that the amplification factor becomes

$$A = \frac{\pi w}{1-e^{-\pi w}}\left|{}_1F_1\left(\frac{1}{2}iw, 1; \frac{1}{2}iwy^2\right)\right|^2, \qquad (6)$$

where ${}_1F_1$ is the confluent hypergeometric function [5, 6].

In the limit of short wavelength ($w \gg 1$), the integrand of Eq. 6 oscillates rapidly and the biggest contribution to the integral comes from stationary points corresponding to geometric optics images. When w is approximately order 1 or larger, the geometric optics approximation breaks down and the wave diffraction effect becomes significant.

Previous microlensing constraints were obtained using observations from the Subaru telescope with the Hyper Suprime Cam (HSC) in the r-band filter [2]. The wavelength of light detectable in this band is comparable to the Schwarzschild radius of a PBH with $M_{PBH} \leq 10^{-11}M_\odot$. As a result, the geometric lensing approximation breaks down and diffraction effects become important. This renders the very low mass range untestable by the HSC. The HSC is sensitive to a microlensing event when the magnification is $A \geq 1.34$. At small values of the dimensionless frequency w, there can be no detectable lensing events; the magnification will always be lower than the threshold as shown by the gray line in Figure 1.

However, we note that the previous microlensing constraints show no appreciable difference between wave and geometric approaches when the finite size effect is taken into account [2, 3]. This is because during a real observation, the diffraction term in Eq. 4 averages out. In this case, the diffraction effects provide only small corrections to the threshold impact parameter found by only considering finite size effects. This is shown in Figure 2. Therefore, in this paper we limit our discussion to the dominant effects of finite source size.

B. Finite Size Effects

The microlensing magnification depends in general on the size of the source [7]. The peak magnification for an extended source can be either smaller or larger than the peak magnification for a point source. The size of the source, along with the magnitude of the impact parameter, determine whether the peak magnification is enhanced or diminished [8]. When the impact parameter becomes small ($u \ll r_{source}$), however, the peak magnification for a point source diverges, while the peak magnification for an extended source remains finite. This means that for PBHs that cross very near the center of our line-of-sight to an extended source, the peak magnification will be significantly lower than in the point source case. We can recalculate the magnification, taking into account the finite size effects following [8] and [3]. Including both finite-source and wave effects, we can see how the amplification changes with source size and wavelength, as shown in Figure 1.

To determine the magnification of a finite-size source, we use the size of the source in the plane of the lensing PBH. Therefore, it is convenient to define the parameter

$$U \equiv \frac{\theta_S}{\theta_E} = \frac{R_S/d_S}{R_E/d_L}, \qquad (7)$$

where θ_S is the angular size of the source.

The finite size effects are most prominent in the regime where $U \gg 1$, but are not negligible even when $U < 1$. The magnification is given by integrating Eq. (3) over the source star in the plane of the lensing PBH

$$A_{finite}(u, U) \equiv \frac{1}{\pi U^2}\int_{|\mathbf{y}|\leq U} d^2\mathbf{y}A_{geo}(|\mathbf{u}-\mathbf{y}|). \qquad (8)$$

Under the geometric approximation Eq. (3), the threshold magnification corresponds to a threshold impact parameter value of $u = 1$. When taking into account the finite size effects, the threshold impact parameter will be different from unity in general. Following the prescription of [3], we can calculate the value of the impact parameter that corresponds to a detectable event by setting $A_{finite} = 1.34$ for a particular set of parameters d_L, M_{PBH}, r_{source}, and solving for u_{thresh} in Eq. (8). The values of u_{thresh} for the cases of a point source, extended source, and extended source with wave effects at a particular distance are shown in Figure 2.

In general, the threshold impact parameter depends both on both d_L and r_{source} In Figure 3, this dependence is explicitly shown for different values of M_{PBH} and r_{source}.

II. SOURCE SIZE REVISITED:

The HSC constraints assume a source size of $R_\odot$ for simplicity [2], but the observations are much more sensitive to significantly larger stars. This can be seen by considering the detection efficiency of the HSC (30-20% for $m_r = 25 - 26$ mag, and 70-60% for $m_r = 23 - 24$ mag). A back-of-the-envelope calculation shows that the Sun would have an apparent magnitude of ≈ 29 mag in

the r-band if it were located at the center of M31. A main sequence star located in M31 would need to have a luminosity much greater than that of the Sun in order for a lensing event to be detectable. This implies that the HSC is more sensitive to larger main-sequence stars in general according to Eq. 9. If the source star were off-main sequence, the finite size effects become much more significant. Therefore, we aim to re-derive the constraints using the population of stars in M31 that were both in the field of view and had light curves that could be successfully recovered by the HSC observations.

We use the catalog of stars from the Panchromatic Hubble Andromeda Treasury (PHAT) survey to find the population of stars in M31 which can have detectable microlensing events [9, 10]. The PHAT survey resolved 117 million individual stars and partially overlaps with the HSC data in the disk region. However, the HSC is unable to resolve the fainter stars from the PHAT catalog. We want to ensure as much coincidence as possible between the PHAT stars and the population of microlensing-detectable stars. We also want stars with well-measured colors as this is how we will determine the size of each star. Therefore, we only use stars with a high signal to noise ratio and sufficient sharpness in each filter as signified by the GST tag, see [9]. This guarantees that we only use those PHAT stars with the best photometry.

We include all GST stars from bricks 7 and higher in our analysis. This selection excludes the bulge of M31 which was saturated in the HSC field of view and was therefore a region where microlensing events could not be recovered. We also do a magnitude cut of $m \leq 26$ in the HST WFC F814W filter since this corresponds to the dimmest stars the HSC could observe in the r band. This preferentially eliminates small stars from our analysis since they will have lower luminosities on average. It should be noted that at many points in the HSC survey, the dimmest stars that could be observed were closer to $m = 24$, so our cuts are quite conservative.

To determine the size of stars in the PHAT catalog, we use the MESA Isochrones and Stellar Tracks (MIST) stellar evolution package [11, 12]. We use the isochrones generated for the non-rotating models in the HST ACS/WFC photometric system. We then compare each PHAT star to all the synthetic MIST stars which share sufficiently similar photometry using a nearest neighbors approach. A MIST star is considered a neighbor if it lies within a distance of 0.025 in "magnitude space" of a PHAT star using the apparent magnitudes of a star in each filter. This cutoff value was selected by calculating the number of PHAT stars with at least one nearest neighbor for various cutoff values. Above ≈ 0.025, the number of stars with at least one neighbor doesn't increase significantly. This indicates that most of the stars that have a similar neighbor have already been found. Through this selection process, we found radius probability distributions for approximately 93% of stars in the PHAT catalog. Of these, the standard deviation of the nearest neighbors was $0.4R_\odot$ or less for 90% of samples. This quality of fit is more than sufficient considering the small effect this uncertainty has on the final results (see Section III for details).

We then use the bolometric luminosity and temperature of each synthetic MIST star to construct a probability distribution for the radius of each PHAT star. This is done by assuming blackbody radiation and using the relationship

$$R = \sqrt{\frac{L_{bol}}{4\pi T^4 \sigma}} \tag{9}$$

where σ is Wien's constant.

Because the MIST isochrones artificially contain a large number of high mass stars, one might worry that the results are biased by synthetic stars that are either unphysical or not comparable to the relevant PHAT population. To offset this effect, we weigh the synthetic stars using the Chabrier initial mass function, which disfavors these high mass stars [13].

We also weigh the data by the implied distance of the synthetic stars. By comparing the distance modulus of the synthetic stars to the real PHAT stars, we can compute how far away the synthetic star would be. By comparing this to the actual distance to an M31 star (770 kpc by assumption), we can determine how good a fit the neighboring synthetic stars are and weigh them accordingly. Both of these weighting schemes are used for the remainder of this paper.

The result is a distribution of stars shown in Figure 4. The first peak around $5R_\odot$ comes from main sequence stars, the most abundant branch. In order facilitate HSC-detectable lensing events, main sequence stars must be significantly more luminous than the Sun. Hence, according to Eq. 9, the stars we're considering are typically larger than the Sun, leading to the observed peak. The second peak around $10R_\odot$ likely stems from the overdensity of red giant branch and asymptotic giant branch stars in the disk of M31 [10, 14]. These stars are more luminous in general, and are therefore more likely to be observable to the HSC. So even though the abundance of smaller stars is greater, it is in fact the larger stars that contribute most to the constraints.

III. CONSTRAINTS ON PBH AS DM:

Following the work of Niikura et all [2], the differential event rate for microlensing of a single star by a PBH is given by

$$\frac{d\Gamma_{PBH}}{d\hat{t}} = 2\frac{\Omega_{PBH}}{\Omega_{DM}} \int_0^{d_s} dd_L \int_0^{U_T} du_{min} \frac{1}{\sqrt{u_T^2 - u_{min}^2}} \frac{\rho_{DM}(d_L)}{M_{PBH} v_c^2(d_L)} v^4 \exp\Big[- \frac{v^2}{v_c^2(d_L)} \Big], \tag{10}$$

where $v = 2R_E\sqrt{u_T^2 - u_{min}^2}/\hat{t}$ is the transverse velocity of the PBH, d_L is the distance to the lensing PBH, and d_S is the distance to the source star.

The duration of observation was 7 hours, of which the greatest sensitivity to detection of events was from 0.07 hours to 3 hours. We integrate over the observation to find the total expected rate of events. Assuming a Poisson distribution for events, we can compare the actual detections to the predicted number of detections.

The stellar population in Figure 4 is sorted into linearly spaced bins up to $20R_\odot$, at which point we use logarithmically spaced bins for the remaining few large, sparsely distributed stars. Constraints are generated by performing the integral in Eq. 10 for each bin. Examples of how the constraints change with source size are shown in Figure 5. The benchmark constraints are then generated by weighting each of these resulting constraints according to the abundance of stars within the corresponding bin. This result is shown in Figure 6.

These benchmark constraints indicate that there still exists a large region of parameter space where there are absolutely no constraints on monochromatic PBHs as DM. The revision to the constraints are significant, especially in the low mass range. This can be understood by looking at how the constraints scale with source radius. For a thorough discussion, see [4]. In brief, if the source radius were to double, in order to keep the same parameter U, the lens would need to be brought closer to the Earth according to:

$$\frac{\theta_S}{\theta_E} = \frac{R_S d_L}{R_E d_S} = R_S\Big(\frac{x}{1-x}\Big)^{1/2} \tag{11}$$

where $x = d_L/d_S$. If x is small, which is a good approximation for low mass PBHs since u_T is 0 unless $d_L \ll d_S$, this corresponds to the lens being brought a factor of 4 closer to the Earth. This, in turn, means that the Einstein radius of the PBH will halve. Since $v \propto R_E$, our rate of observed lensing events will go down by a factor of $1/2^6 = 1/64$ for low mass PBHs [4]. This explains why in the low mass regime, the finite size effects can change by such a large margin for a relatively small change in R_S.

The finite size effects also weaken the constraints for intermediate mass black holes. This can be understood by realizing that the finite size effects are greatest when the lensing PBH is close to the source star. That is, as d_L approaches d_S, the finite size effect washes out magnification for all masses of PBH. This is also the region where the DM density contribution from M31 in Eq. 10 is the greatest, leading to a noticeable weakening of the constraints for all but the high mass region of the relevant parameter space.

The uncertainty in the estimation of the radius of each star is shown in the gray shading. The lower bound of this region assumes that the true radius for each PHAT star is that of the smallest nearest neighbor given by the MIST comparison. Similarly, the upper bound of this region assumes that each PHAT star is the that of the largest nearest neighbor given by the MIST comparison. The black line is the benchmark constraint which assumes the radius of each PHAT star is given by the mean of the radii of its nearest neighbors. In the high mass region, the uncertainty in the constraint is minuscule. This is because the finite size effects are less important in this region so the difference in source size has little effect. At lower masses, the uncertainty is noticeable, but still small. This is because when using the minimum estimate for the size of a source star, any given bin will lose some number of stars to a smaller bin, but will also gain a number of stars from a larger bin. The net effect is slight, but reassuring as it suggests that the number and size of bins matters much less than the overall shape of the distribution of stars.

IV. CONCLUSION:

Further work needs to be done to improve the mass range probable by microlensing, increase the sensitivity of observations, and determine the most prudent target of our searches. In general, we would want to observe the greatest number of stars for the longest amount of time. We would also want to observe with a high enough cadence to detect the shortest duration lensing events. Using a shorter wavelength filter to mitigate wave effects would also expand the probable region as suggested by [3].

As shown in this work, the observed stars need to be luminous enough in the band of observation to obtain a sufficient expected number of events. Additionally, isolating sources with smaller radii and observing very far away sources would limit the finite size effects and improve constraints. But this proves challenging when trying to isolate individual stars and achieve the best possible image resolution. Indeed, finding the ideal candidates for observation is a critical step to improving microlensing constraints and is a subject of our future work.

ACKNOWLEDGMENTS

We would like to thank Kevin McKinnon for his assistance in calculating and appropriately weighing the distribution of stellar size in M31.

[1] Andrey Katz, Joachim Kopp, Sergey Sibiryakov, and Wei Xue. Femtolensing by Dark Matter Revisited. *Journal of Cosmology and Astroparticle Physics*, 2018(12):005–005,

December 2018. arXiv: 1807.11495.

[2] Hiroko Niikura, Masahiro Takada, Naoki Yasuda, Robert H. Lupton, Takahiro Sumi, Surhud More, Toshiki Kurita, Sunao Sugiyama, Anupreeta More, Masamune Oguri, and Masashi Chiba. Microlensing constraints on primordial black holes with the Subaru/HSC Andromeda observation. *Nature Astronomy*, 3(6):524–534, June 2019. arXiv: 1701.02151.

[3] Sunao Sugiyama, Toshiki Kurita, and Masahiro Takada. Revisiting the wave optics effect on primordial black hole constraints from optical microlensing search. *arXiv:1905.06066 [astro-ph]*, May 2019. arXiv: 1905.06066.

[4] Paulo Montero-Camacho, Xiao Fang, Gabriel Vasquez, Makana Silva, and Christopher M. Hirata. Revisiting constraints on asteroid-mass primordial black holes as dark matter candidates. *arXiv:1906.05950 [astro-ph]*, June 2019. arXiv: 1906.05950.

[5] Takahiro T. Nakamura and Shuji Deguchi. Wave Optics in Gravitational Lensing. *Progress of Theoretical Physics Supplement*, 133:137–153, January 1999.

[6] Ryuichi Takahashi and Takashi Nakamura. Wave Effects in the Gravitational Lensing of Gravitational Waves from Chirping Binaries. *The Astrophysical Journal*, 595(2):1039–1051, October 2003.

[7] Norihito Matsunaga and Kazuhiro Yamamoto. The finite source size effect and wave optics in gravitational lensing. *Journal of Cosmology and Astroparticle Physics*, 2006(01):023–023, January 2006.

[8] Hans J. Witt and Shude Mao. Can lensed stars be regarded as pointlike for microlensing by MACHOs? *The Astrophysical Journal*, 430:505–510, August 1994.

[9] Benjamin F. Williams, Dustin Lang, Julianne J. Dalcanton, Andrew E. Dolphin, Daniel R. Weisz, Eric F. Bell, Luciana Bianchi, Nell Byler, Karoline M. Gilbert, Lo Girardi, Karl Gordon, Dylan Gregersen, L. C. Johnson, Jason Kalirai, Tod R. Lauer, Antonela Monachesi, Philip Rosenfield, Anil Seth, and Eva Skillman. THE PANCHROMATIC HUBBLE ANDROMEDA TREASURY. X. ULTRAVIOLET TO INFRARED PHOTOMETRY OF 117 MILLION EQUIDISTANT STARS. *The Astrophysical Journal Supplement Series*, 215(1):9, October 2014.

[10] Julianne J. Dalcanton, Benjamin F. Williams, Dustin Lang, Tod R. Lauer, Jason S. Kalirai, Anil C. Seth, Andrew Dolphin, Philip Rosenfield, Daniel R. Weisz, Eric F. Bell, Luciana C. Bianchi, Martha L. Boyer, Nelson Caldwell, Hui Dong, Claire E. Dorman, Karoline M. Gilbert, Lo Girardi, Stephanie M. Gogarten, Karl D. Gordon, Puragra Guhathakurta, Paul W. Hodge, Jon A. Holtzman, L. Clifton Johnson, Sren S. Larsen, Alexia Lewis, Jason L. Melbourne, Knut A. G. Olsen, Hans-Walter Rix, Keith Rosema, Abhijit Saha, Ata Sarajedini, Evan D. Skillman, and Krzysztof Z. Stanek. THE PANCHROMATIC HUBBLE ANDROMEDA TREASURY. *The Astrophysical Journal Supplement Series*, 200(2):18, May 2012.

[11] Jieun Choi, Aaron Dotter, Charlie Conroy, Matteo Cantiello, Bill Paxton, and Benjamin D. Johnson. Mesa Isochrones and Stellar Tracks (MIST). I. Solar-scaled Models. *The Astrophysical Journal*, 823:102, June 2016.

[12] Aaron Dotter. MESA Isochrones and Stellar Tracks (MIST) 0: Methods for the Construction of Stellar Isochrones. *The Astrophysical Journal Supplement Series*, 222:8, January 2016.

[13] Gilles Chabrier. Galactic Stellar and Substellar Initial Mass Function. *Publications of the Astronomical Society of the Pacific*, 115:763–795, July 2003.

[14] Karl D. Gordon, Morgan Fouesneau, Heddy Arab, Kirill Tchernyshyov, Daniel R. Weisz, Julianne J. Dalcanton, Benjamin F. Williams, Eric F. Bell, Luciana Bianchi, Martha Boyer, Yumi Choi, Andrew Dolphin, Leo Girardi, David W. Hogg, Jason S. Kalirai, Maria Kapala, Alexia R. Lewis, Hans-Walter Rix, Karin Sandstrom, and Evan D. Skillman. The Panchromatic Hubble Andromeda Treasury XV. The BEAST: Bayesian Extinction and Stellar Tool. *The Astrophysical Journal*, 826(2):104, July 2016. arXiv: 1606.06182.

[15] Yacine Ali-Hamoud and Marc Kamionkowski. Cosmic microwave background limits on accreting primordial black holes. *Physical Review D*, 95(4):043534, February 2017.

[16] Yacine Ali-Hamoud and Marc Kamionkowski. Cosmic microwave background limits on accreting primordial black holes. *Physical Review D*, 95(4):043534, February 2017.

[17] Leandro G. Althaus, Alejandro H. Crsico, Jordi Isern, and Enrique Garca-Berro. Evolutionary and pulsational properties of white dwarf stars. *The Astronomy and Astrophysics Review*, 18(4):471–566, October 2010. arXiv: 1007.2659.

[18] B. J. Carr and S. W. Hawking. Black Holes in the Early Universe. *Monthly Notices of the Royal Astronomical Society*, 168(2):399–415, August 1974.

[19] Vera C. Rubin and W. Kent Ford. Rotation of the Andromeda Nebula from a Spectroscopic Survey of Emission Regions. *The Astrophysical Journal*, 159:379, February 1970.

[20] F. Zwicky. On the Masses of Nebulae and of Clusters of Nebulae. *The Astrophysical Journal*, 86:217, October 1937.

[21] Puragra Guhathakurta, Brian Yanny, Donald P. Schneider, and John N. Bahcall. Globular cluster photometry with the Hubble Space Telescope. I - Description of the method and analysis of the core of 47 TUC. *The Astronomical Journal*, 104:1790–1817, November 1992.

[22] Ahmed Alhamzawi and Rahim Alhamzawi. Gravitational lensing in the strong field limit by modified gravity. *General Relativity and Gravitation*, 48(12):167, December 2016.

[23] Lus C. B. Crispino, Sam R. Dolan, and Ednilton S. Oliveira. Electromagnetic Wave Scattering by Schwarzschild Black Holes. *Physical Review Letters*, 102(23):231103, June 2009.

[24] Takahiro T. Nakamura. Gravitational Lensing of Gravitational Waves from Inspiraling Binaries by a Point Mass Lens. *Physical Review Letters*, 80(6):1138–1141, February 1998.

[25] Shuji Deguchi and William D Watson. DIFFRACTION IN GRAVITATIONAL TENSING FOR COMPACT OBJECTS OF LOW MASS. *ApJ. . .*, 307:8.

[26] V. Bozza. Gravitational lensing in the strong field limit. *Physical Review D*, 66(10):103001, November 2002. arXiv: gr-qc/0208075.

[27] Yang Bai and Nicholas Orlofsky. Microlensing of X-ray Pulsars: a Method to Detect Primordial Black Hole Dark Matter. *arXiv:1812.01427 [astro-ph, physics:hep-ph]*, November 2018. arXiv: 1812.01427.

[28] Misao Sasaki, Teruaki Suyama, Takahiro Tanaka, and Shuichiro Yokoyama. Primordial Black Holes - Perspectives in Gravitational Wave Astronomy -. *Classical and Quantum Gravity*, 35(6):063001, March 2018. arXiv: 1801.05235.

[29] Keisuke Inomata, Masahiro Kawasaki, Kyohei Mukaida, and Tsutomu T. Yanagida. Double inflation as a single origin of primordial black holes for all dark matter and LIGO observations. *Physical Review D*, 97(4):043514, February 2018. arXiv: 1711.06129.

[30] Anne M. Green. Microlensing and dynamical constraints on primordial black hole dark matter with an extended mass function. *Physical Review D*, 94(6):063530, September 2016. arXiv: 1609.01143.

[31] L. Clifton Johnson, Anil C. Seth, Julianne J. Dalcanton, Lori C. Beerman, Morgan Fouesneau, Alexia R. Lewis, Daniel R. Weisz, Benjamin F. Williams, Eric F. Bell, Andrew E. Dolphin, Sren S. Larsen, Karin Sandstrom, and Evan D. Skillman. Panchromatic Hubble Andromeda Treasury XVI. Star Cluster Formation Efficiency and the Clustered Fraction of Young Stars. *The Astrophysical Journal*, 827(1):33, August 2016. arXiv: 1606.05349.

[32] Benjamin F. Williams, Julianne J. Dalcanton, Eric F. Bell, Karoline M. Gilbert, Puragra Guhathakurta, Tod R. Lauer, Anil C. Seth, Jason S. Kalirai, Philip Rosenfield, and Leo Girardi. THE PANCHROMATIC HUBBLE ANDROMEDA TREASURY. II. TRACING THE INNER M31 HALO WITH BLUE HORIZONTAL BRANCH STARS. *The Astrophysical Journal*, 759(1):46, November 2012.

[33] Philip Rosenfield, L. Clifton Johnson, Lo Girardi, Julianne J. Dalcanton, Alessandro Bressan, Dustin Lang, Benjamin F. Williams, Puragra Guhathakurta, Kirsten M. Howley, Tod R. Lauer, Eric F. Bell, Luciana Bianchi, Nelson Caldwell, Andrew Dolphin, Claire E. Dorman, Karoline M. Gilbert, Jason Kalirai, Sren S. Larsen, Knut A. G. Olsen, Hans-Walter Rix, Anil C. Seth, Evan D. Skillman, and Daniel R. Weisz. THE PANCHROMATIC HUBBLE ANDROMEDA TREASURY. I. BRIGHT UV STARS IN THE BULGE OF M31. *The Astrophysical Journal*, 755(2):131, August 2012.

[34] Stphane Courteau, Lawrence M. Widrow, Michael McDonald, Puragra Guhathakurta, Karoline M. Gilbert, Yucong Zhu, Rachael Lynn Beaton, and Steven R. Majewski. THE LUMINOSITY PROFILE AND STRUCTURAL PARAMETERS OF THE ANDROMEDA GALAXY. *The Astrophysical Journal*, 739(1):20, September 2011.

[35] Juan Garca-Bellido and Sebastien Clesse. Constraints from microlensing experiments on clustered primordial black holes. *arXiv:1710.04694 [astro-ph, physics:gr-qc, physics:hep-th]*, October 2017. arXiv: 1710.04694.

[36] Sunao Sugiyama, Toshiki Kurita, and Masahiro Takada. Revisiting the wave optics effect on primordial black hole constraints from optical microlensing search. *arXiv:1905.06066 [astro-ph]*, May 2019. arXiv: 1905.06066.

[37] Juan Garca-Bellido and Sebastien Clesse. Constraints from microlensing experiments on clustered primordial black holes. *arXiv:1710.04694 [astro-ph, physics:gr-qc, physics:hep-th]*, October 2017. arXiv: 1710.04694.

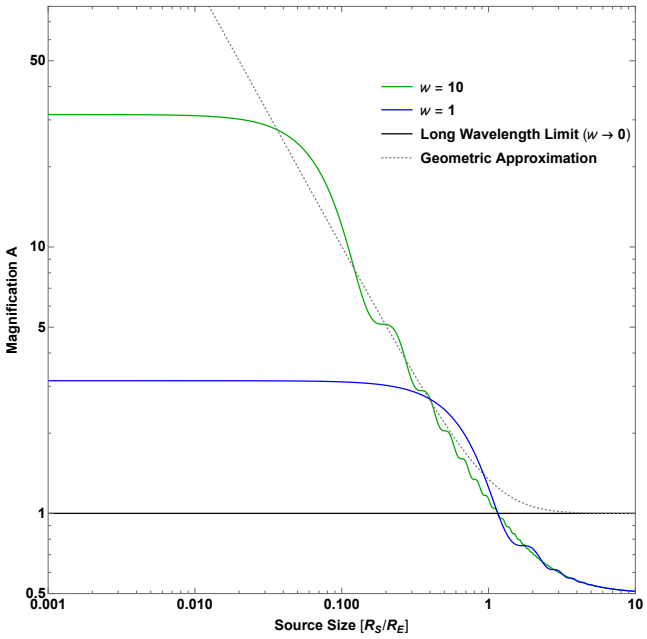

Figure 1. The magnification for different values of the dimensionless frequency w. In the geometric approximation, shown in dotted gray, the wave effects of light are ignored and the magnification is independent of the source size. In the long wavelength limit, shown in solid gray, the light effectively ignores the lens and no magnification occurs. For $w \geq 1$, the the magnification increases as source size decreases, but reaches a maximum at πw.

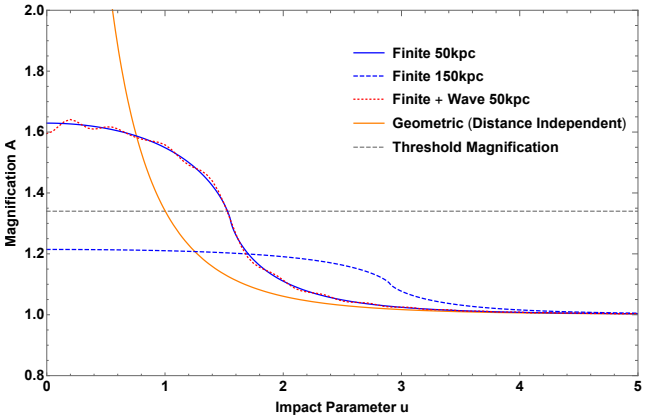

Figure 2. The threshold impact parameter values for geometric, finite, and finite + wave models with a source star of radius $R_\odot$. In the geometric approximation, the threshold impact parameter is always 1, regardless of lens distance. When including finite size effects, the threshold impact parameter now depends on distance. If we move the lens further away, that is, closer to the source star, at a certain distance there will no longer be any detectable magnification as shown by the dashed blue line. The wave effects, shown in red, are small corrections to the finite size effects and are thus not considered further for the purposes of this paper.

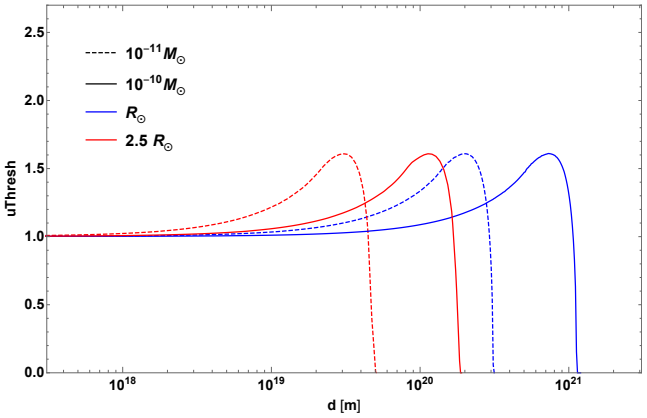

Figure 3. The dependence of the threshold impact parameter on M_{PBH} and r_{source}. For larger stars, the finite size effects become important at a smaller distance. Similarly, for lighter PBHs, the finite size effects are more dominant. Considering the population of stars in M31, this results in little to no detectable magnification for PBHs close to M31 unless they are well above asteroid mass.

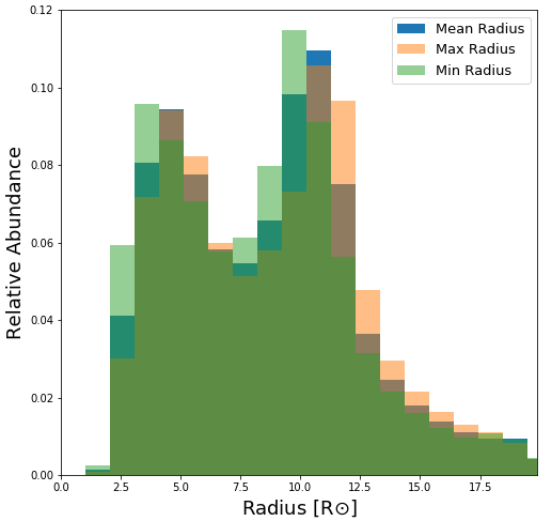

Figure 4. The Population of Stars in M31 which could have microlensing light curves resolvable by the HSC survey. Larger stars tend to have greater total luminosity in general and are therefore the easiest to detect. The assumption of $R_{source} = R_{\odot}$ significantly underestimates the impact of finite size effects. The blue histogram shows the values used for our benchmark constraints. The uncertainty estimation comes from using the largest or smallest radius estimate for each star. See Section II for details.

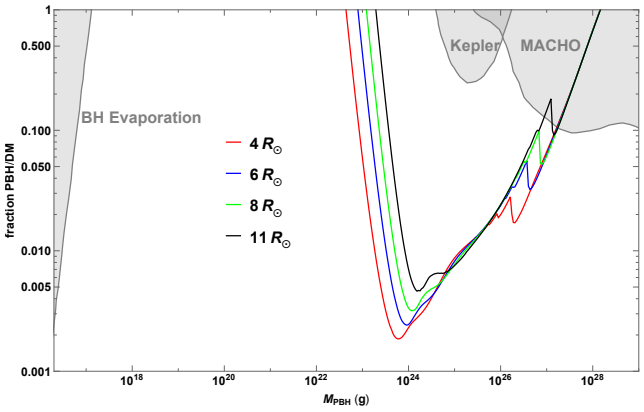

Figure 5. The constraints for each individual Radius of a source star. The jagged feature arises from the point at which the DM density contribution from PBH in M31 in Eq. 10 becomes negligible. Lower mass PBHs must be located close to the Milky Way in order to facilitate a detectable lensing event. The sharpness of this feature is averaged out in the benchmark constraints.

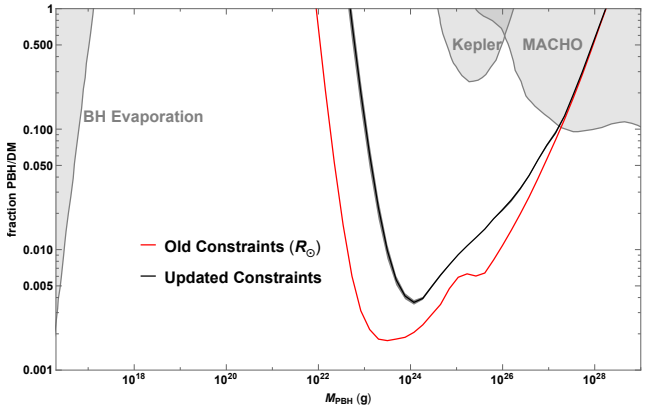

Figure 6. The constraints on primordial black holes as dark matter. The black line is the benchmark constraint and the primary result of this paper. The gray shading comes from the uncertainty in determining the stellar size distribution. The red line is the previous constraint which includes finite size effects, but assumes that all stars in M31 have a radius of $R_\odot$.

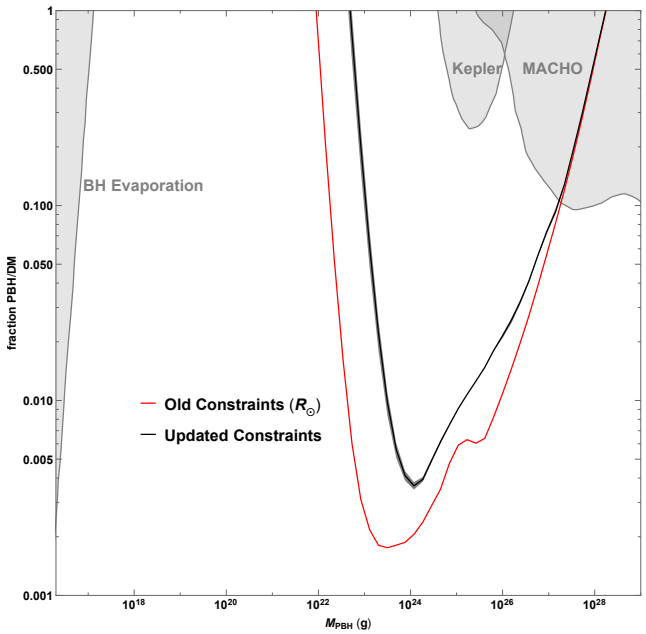

Figure 7. Square Benchmark

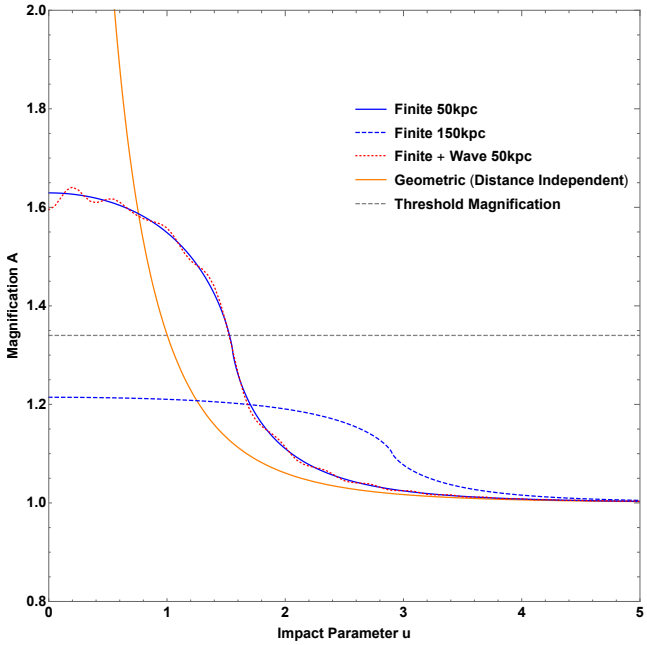

Figure 8. Square MagImpact

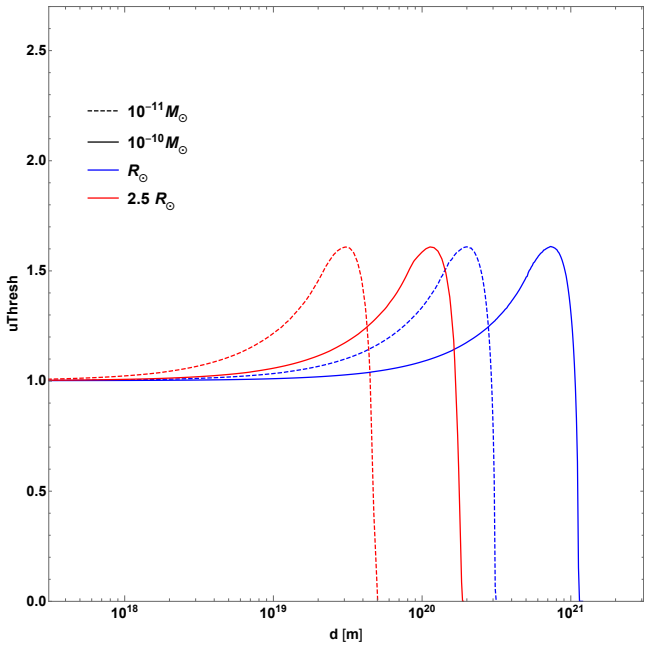

Figure 9. Square DistImpact

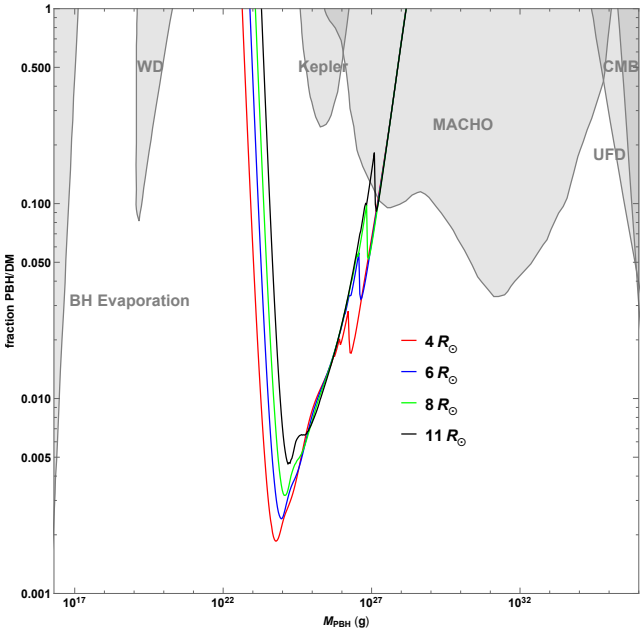

Figure 10. Square Comparison Constraints